Husformer: A Multi-Modal Transformer for Multi-Modal Human State Recognition

Ruiqi Wang†, Wonse Jo†, Dezhong Zhao, Weizheng Wang, Baijian Yang, Guohua Chen and Byung-Cheol Min

Abstract—Human state recognition is a critical topic with pervasive and important applications in human-machine systems. Multi-modal fusion, the combination of metrics from multiple data sources, has been shown as a sound method for improving the recognition performance. However, while promising results have been reported by recent multi-modal-based models, they generally fail to leverage the sophisticated fusion strategies that would model sufficient cross-modal interactions when producing the fusion representation; instead, current methods rely on lengthy and inconsistent data preprocessing and feature crafting. To address this limitation, we propose an end-to-end multi-modal transformer framework for multi-modal human state recognition called *Husformer*. Specifically, we propose to use cross-modal transformers, which inspire one modality to reinforce itself through directly attending to latent relevance revealed in other modalities, to fuse different modalities while ensuring sufficient awareness of the cross-modal interactions introduced. Subsequently, we utilize a self-attention transformer to further prioritize contextual information in the fusion representation. Using two such attention mechanisms enables effective and adaptive adjustments to noise and interruptions in multi-modal signals during the fusion process and in relation to high-level features. Extensive experiments on two human emotion corpora (DEAP and WESAD) and two cognitive workload datasets (MOCAS and CogLoad) demonstrate that in the recognition of human state, our *Husformer* outperforms both state-of-the-art multi-modal baselines and the use of a single modality by a large margin, especially when dealing with raw multi-modal signals. We also conducted an ablation study to show the benefits of each component in *Husformer*.

Index Terms—Affective and Cognitive State Recognition, Multi-modal Fusion, Multi-modal Deep Learning, Transformer

1 Introduction

 ${f R}$ ECOGNITION of human state, including human affective state, known as emotion, and cognitive workload, known as mental stress, plays an enormous role in any human-machine interaction systems, as enabling machines to perceive, understand, and adapt to different human emotional and cognitive states, and improves the performance of the whole systems [1], [2], [3]. Generally, human state assessment methods can be categorized into two mainstreams according to the signal types utilized: physiological assessments perceive human physiological metrics, such as galvanic skin response (GSR), electroencephalography (EEG), electrooculography (EOG), electrocardiography (ECG), electromyogram (EMG), and heart rate (HR), which fluctuate according to unintentional reactions of the human nervous system under a certain human state; behavioral assessments analyze unconscious human behavioral responses, such as facial expressions, body and eye movements, and mouse movements, and relate them to different types of human states [4].

Unfortunately, owing to the complexity of human state reasoning, it is improbable that signals from a single modal-

Manuscript received.

ity are sufficient to achieve optimal recognition performance in terms of accuracy and robustness [5], [6], [7]. For instance, different signals possess different levels of sensitivity to different task environments and even different human subjects, and determining one modality that is efficient for every task scenario and subject is impractical and impossible. Furthermore, reliance on a unimodal data source means that noise or interruption of signal can result in extensive error or even failure of the recognition system [8].

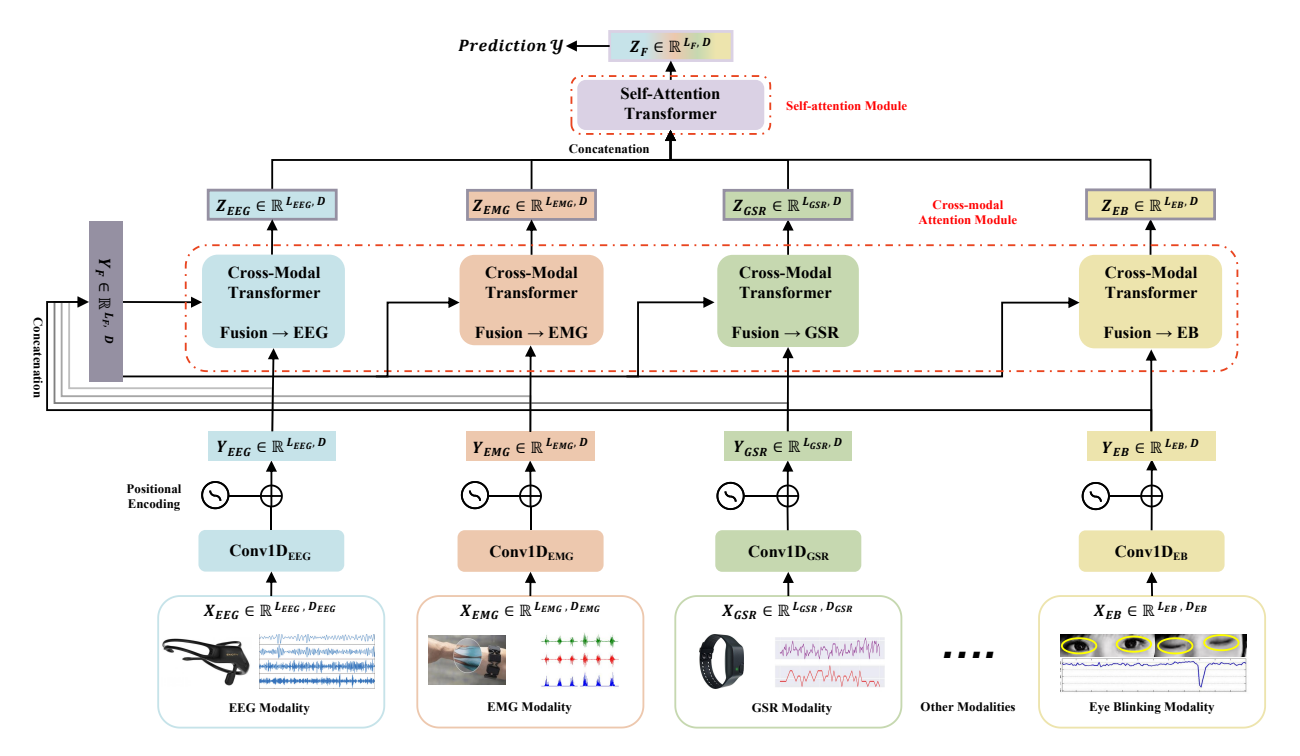
Recently, multi-modal fusion-based human state recognition methods that combine data from multiple modalities have been proposed and demonstrated promise as a solution for the aforementioned challenges faced by single-modal-based approaches [9], [10], [11], [12], [13]. The adoption of multi-modal signals can reduce the noise-to-signal ratio and enhance tolerance against sensor failures. Moreover, fusing different metrics collected from the same subject under one particular human state through multiple modalities can reveal important and comprehensive features of human emotion and cognitive workload that are inaccessible via a single modality [5], [7].

However, existing multi-modal fusion models for human state recognition are still in very preliminary stages and have several drawbacks. To start with, the high redundancy, noise, and collinearity in multi-modal raw data [27] necessitate extensive preprocessing (data cleaning and feature crafting) before the classification model in order to achieve reasonable performance [28], [29], [30]. Also, different modalities are usually preprocessed by different methods, and the parameters of those methods must be carefully selected through cross-validation to be optimal

R.Q. Wang, W. Jo, W.Z. Wang, B.J Yang and B.-C. Min are with the Department of Computer and Information Technology, Purdue University, West Lafayette, IN 47907, USA (e-mail: [wang5357, jow, wang5716, byang, minb] @purdue.edu).

D.Z. Zhao and G.H. Chen are with College of Mechanical and Electrical Engineering, Beijing University of Chemical Technology, Beijing, China, (e-mail: DZ_Zhao@buct.edu.cn, chengh@mail.buct.edu.cn).

^{• †:} equal contribution



[22]. Such lengthy and inhomogeneous preprocessing undermines the simplicity of the model and its applicability to new task scenarios. Furthermore, most multi-modal fusion methods tend to produce the fusion representation through directly concatenating different modalities despite them being incommensurable and having unbalanced spatial and temporal feature dimensions [5]. Such direct fusion schemes ignore the latent correlations across modalities and may be limited by non-instantaneous coupling and the curse of dimensionality [31]. As a result, most such models do not show statistically significant improvements in accuracy over single-modal ones, especially EEG-based unimodal approaches [5], [7]. While several methods have been proposed of late to learn cross-modal interactions by training shared representations [13], [19], [20], their network structures are too shallow to capture complicated cross-modal correlations and introduce sufficient complementarity across different modalities, particularly when dealing with raw multimodal signals that are interrupted by noise and artifacts. In addition, to our best knowledge, none of the existing multi-modal methods focuses on and has been shown to effectively predict both human affective state and cognitive workload, and most are tailored for a specific combination of modalities under certain task scenarios, leading to a deficiency of generality.

To address aforementioned issues, we present *Husformer*: a multi-modal transformer for multi-modal human state recognition and an end-to-end model that learns representations of human state directly and efficiently from raw multimodal data streams. Figure 1 demonstrates its structure with four example input modalities: EEG, EMG, GSR and eye blinking (EB). The core components of Husformer are the cross-modal attention module and self-attention module, which respectively consist of multiple cross-modal attention transformers and one self-attention transformer. The crossmodal attention transformers model the latent interactions across modalities, continuously adapting and reinforcing features from one modality with those of other modalities (e.g., EEG ← EMG, GSR, and EB). Unlike direct concatenation of multi-modal modalities or learning cross-modal shared representations through shallow neural networks, our cross-modal attention mechanism encourages the target modality to directly attend to low-level features in other modalities where strongly relevant and complementary information is revealed, leading to more adaptive and efficient complementarity and cooperation across multiple modalities. The self-attention transformer then prioritizes the important contextual information in the fusion representation concatenated from reinforced unimodal features of all modalities supplied by the cross-modal attention

TABLE 1: Comparison of the *Husformer* with existing methods for multi-modal human state recognition.

Paper	Year	Target Human State	Validation Dataset (Stimuli)	Modalities	Preprocessing Procedures	Classification Model (*: best performing)
[14]	2010	Cognitive Workload	Non-public (Driving Simulation)	EEG, GSR, PPG, RESP	FFS, MAF, LPF	SVM
[15]	2014	Cognitive Workload	Non-public (N-back Game)	EEG, GSR, RESP, EOG	HPF, LPF, FOSMT, FFT, GBW	SVM*
[13]	2017	Emotion	SEED [16], Preprocessed DEAP [17]		HW, DE, LPF, Statistical feature selection, \sim	BDA + LSTM
[18]	2017	Cognitive Workload	Non-public (N-back Game)	EEG, ECG	BF, CoW, Statistical feature selection	SVM*
[19]	2018	Emotion	Non-public (Film Clips)	EEG, Eye movements	PCA, FFT	BDA + SVM
[20]	2018	Emotion	SEED [16], Preprocessed DEAP [17]		HW, DE, Statistical Feature Selection, \sim	DCCA + SVM
[21]	2019	Emotion	Preproceesed DEAP [17]		~	MMResLSTM
[22]	2020	Cognitive Workload	Non-public (Robot-assisted surgery)	EEG, GSR, HRV, EMG	IIR, HW, FFT, ICA, Statistical feature selection	SVM*
Ours	2022	Cognitive Workload and Emotion	DEAP [17], WESAD [23], MOCAS [24], CogLoad [25]		Not Required	Husformer

Explanation of Acronyms: Photoplethysmography (PPG), Respiration (RESP), Blood Volume Pulse (BVP), Forward Feature Selection (FFS), Moving Average Filter (MAF), Low Pass Filter (LPF), High Pass Filter (HPF), FieldTrip Open Source MATLAB Toolbox (FOSMT), Fast Fourier Transform (FFT), Gaussian Blurring Window (GBW), Hanning Window (HW), Coiflet Wavelet (CoW), Butterworth Filter (BF), Differential Entropy (DE), Principal Component Analysis (PCA), Infinite Impulse Response (IIR), Independent Component Analysis (ICA), Support Vector Machine (SVM), Bimodal Deep Autoencoder (BDA)[26], Long Short-Term Memory network (LSTM), Multimodal Residual LSTM (MMResLSTM), Deep Canonical Correlation Analysis (DCCA). · · · : modalities contained in the public datasets; and ~: preprocessing procedures conducted in the preprocessed public datasets.

transformers, and finally generates a weighted high-level fusion representation based on which predictions are made.

To evaluate *Husformer*, we performed extensive experiments utilizing two multi-modal emotion datasets, DEAP [17] and WESAD [23], and two multi-modal cognitive workload datasets, MOCAS [24] and CogLoad [25]. We also conducted a comprehensive ablation study to investigate the benefits of each module in *Husformer*.

The main contributions of this work can be summarized as follows:

- Husformer is an end-to-end model that learns directly and efficiently from raw multi-modal physiological and behavioral signals generated by sensors, without the massive data preprocessing and feature crafting required in previous works.
- We introduce cross-modal attention transformers to fuse features from different modalities and sufficiently model cross-modal interactions, and then a self-attention transformer to prioritize effectual contextual information in the fusion representation.
- For the first time, we present a generic model for human state recognition, proven to be effective for both human emotion and cognitive workload.
- Our extensive experiments on four publicly available datasets demonstrate the benefits of the *Husformer* and each of its constituent modules.

2 BACKGROUND

This section reviews existing research on human state recognition using multi-modal fusion approaches and the preliminary transformer networks that serve as the basis of our model.

2.1 Multi-Modal Fusion for Human State Recognition

Given the complex nature of human state, a single modality is insufficient to achieve recognition with satisfactory performance in terms of accuracy and robustness, especially in real-world task scenarios where signals are more subject to interruption, noise, and delay [5], [7]. To solve this issue, we utilized a fusion of multiple modalities, integrating data from more than one source modality into a synchronized compact representation and considering the correlations across different modalities. The advantages of multi-modal fusion have already been exploited in various fields such as autonomous vehicles [32], natural language processing [33], scene recognition [34], and weather forecasting [35].

While multi-modal fusion methods for human state recognition also exist, they are still at quite initiatory stages of development and suffer from key defects in data processing and fusion. First of all, for most existing works, the abundant collinearity, noise, and artifacts in raw multimodal data necessitate considerable preprocessing and feature crafting upstream of the classification model to reach sound performance. In addition, different modalities are usually preprocessed by different methods whose optimal parameters are initially unknown. For example, in [36], infinite impulse response (IIR) high-pass and Hanning window filters were used for EEG modality data preprocessing while continuous decomposition analysis and other physiological libraries were utilized for GSR and HR modalities. Afterwards, independent component analysis (ICA) and feature selection procedures depending on prior knowledge were adopted to preprocess candidate features a second time. Such involved non-uniform preprocessing procedures harm the simplicity and universality of the model, making it difficult to apply to general task scenarios and especially to realistic applications, which runs counter to the original intention of multi-modal fusion.

Moreover, while the direct concatenation of different modalities at sensor, feature, or decision level has been widely adopted in prior research [37], [15], [18], [22], [38], this may result in meaningless added information or even bias and noise owing to the feature noncommensurability and different sensitivity of different modalities. For instance, simply fusing HR with other modalities can introduce additional valuable information in some task scenarios but bring disruption in others, as HR-related signals are not only influenced by cognitive workload and emotion but also by irrelevant physical activities [5]. In addition, directly fusing different modalities whose features have unbalanced length and temporal dimensions can lead to non-instantaneous coupling even when they are manually synchronized. In general, simple concatenation operations fail to model the cross-modal interactions and thus are unlikely to capture important representations that would otherwise be revealed by multi-modal fusion.

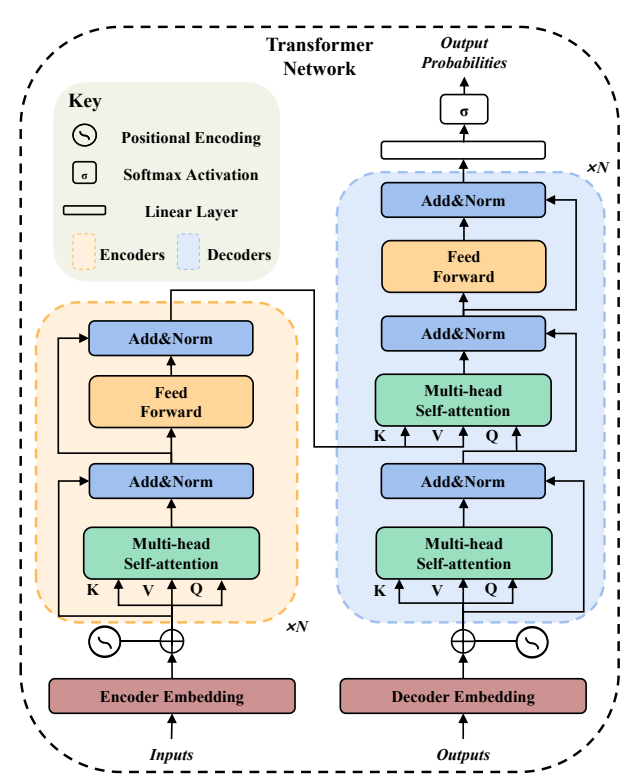
Lately, some advanced fusion schemes have been proposed to solve the above issues; these aim to model crossmodal interactions by training shared representations across different modalities. For example, [13] adopts restricted Boltzmann machines (RBM) [26] to train a hidden layer that is expected to learn the shared representations of sublayers from different modalities; [39] introduces cross-modal temporal correlations obtained via learning shared weights across sub-layers of different modalities; and [20] utilizes deep canonical correlation analysis (DCCA) [40] to maximize the correlations among features of two modalities. However, due to their utilization of shallow network structures, these existing methods are unlikely to comprehensively capture tangled correlations across different modalities, especially from raw multi-modal signals where features are more interrupted. Moreover, the DCCA utilized in [20] can only analyze the correlation between two modalities, limiting the application of the model to general task scenarios that may require the simultaneous fusion of more than two modalities.

Additionally, as far as we know, existing works only focus on the recognition of either affective state or cognitive state, and most are tailored for specific task scenarios and not validated on publicly available datasets; thus the models lack generality and replicability.

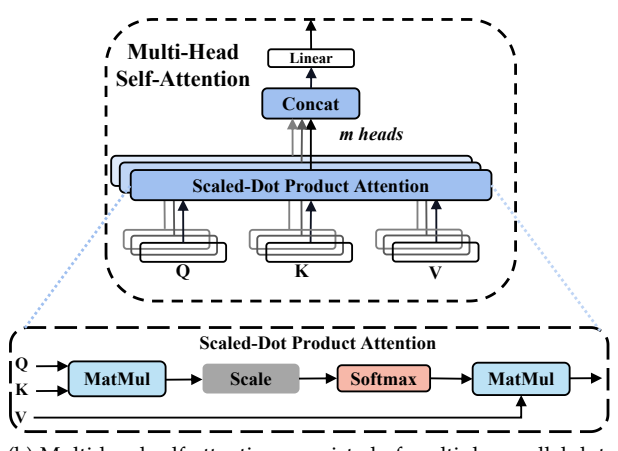
The details of existing works in multi-modal fusion for human state recognition are summarized in Table 1. Distinct from these prior studies, our proposed *Husformer* 1) focuses on general recognition of human state, including emotion and cognitive workload; 2) does not require any data preprocessing and feature crafting procedures, but rather learns from multi-modal raw data series; and 3) utilizes cross-modal attention transformers as the fusion strategy, thereby introducing efficient cooperation and complementary adaptions across modalities regardless of the number of modalities.

2.2 Transformer Network Overview

The transformer network was originally proposed by [41] to solve sequence-to-sequence machine translation tasks in the natural language processing area. As depicted in Figure 2a, a transformer network takes on an encoder-to-decoder



(a) Transformer network: stacked by multiple encoder and decoder layers.



(b) Multi-head self-attention: consisted of multiple parallel dot-product attention blocks [41]. MatMul: matrix multiplication.

Fig. 2: Illustration of the transformer network and multi-head self-attention.

structure, where the encoder and decoder are comprised of multiple identical blocks. The encoder extracts features of the input sequence and provides sufficient contextual information for the decoder, while the decoder generates a prediction of the next element in the output sequence using the incorporated contextual information and the predicted previous element. The encoder is usually executed once, while the decoder is executed until all elements in the output sequence have been generated. Distinct from the traditional encoder-to-decoder structure, the transformer network adopts a multi-head self-attention mechanism to substitute for the attention-based convolution and recurrence layers. The core components in a transformer network

are described in following sub-sections, and readers are referred to [41] for more details.

2.2.1 Embedding Layers and Positional Encoding

The function of an embedding layer, e.g., encoder embedding and decoder embedding, is to transform raw input data such as text and images into a vector representation that can be processed by the transformer network. Due to the lack of convolutions and recurrence layers, a transformer network is order-invariant, lacking the positional information of the input sequence, i.e., the position of each entity in the sequence. Therefore, to provide time-related sequential information for the model, positional encoding (PE) is executed after embedding layers; this augments each entity in the input sequence with an extra positional vector. PE can be implemented in many ways, including using a fixed function [41], such as sin and cos functions in different frequencies, and being set as a learnable parameter [42], [43].

2.2.2 Multi-head Self-attention

Self-attention is an attention mechanism that aims to calculate a global representation of a sequence input that reveals meaningful contextual information by relating different components within the sequence. Basically, a self-attention block adapts each entity in a sequence by considering the global contextual information of the whole sequence [44]. Multi-head self-attention splits the attention into multiple latent sub-spaces (heads), which enables modeling of multiple complex contextual relations across elements in the sequence, leading to a more comprehensive global representation.

Figure 2b illustrates the multi-head self-attention process. Let $X \in \mathbb{R}^{N,D}$ present a sequence consisting of N elements $(x_1,...,x_n)$, where D is the feature dimension of each element. The multi-head self-attention is expected to encapsulate the contextual interactions across these N elements from multiple respects to generate the global representation. This goal is achieved by learning three groups of defined weight matrices: $W_{Q_1,\ldots,m}\in\mathbb{R}^{D,D_Q}$, $W_{K_1,\ldots,m}\in\mathbb{R}^{D,D_K}$, and $W_{V_1,\ldots,m}\in\mathbb{R}^{D,D_V}$, where m presents the head number. In self-attention layer of each head, a scaled-dot product attention is executed in parallel. To begin with, in the i^{th} head self-attention layer, the input sequence $X \in \mathbb{R}^{N,D}$ is mapped separately onto three weight matrices: W_{Q_i} , W_{K_i} and W_{V_i} , to produce projections: Querys Q_i , Keys K_i and Values V_i . Then the attention score sum S_i of each element pair in the sequence is calculated by $S_i = Q_i \cdot K_i^{\top}$. Such an attention score decides the attention degree to be given to other entities when updating and encoding the entity at the current position of the sequence. Furthermore, the attention score S_i is scaled by: $\hat{S}_i = S_i / \sqrt{D_K}$, to improve the stability of gradient iteration. The normalized attention score \hat{S}_i is then translated into probabilities P_i by a softmax function: $P_i = softmax(S_i)$. Finally, the output $head_i$ embedded with weighted attention values is computed by: $head_i = P_i \cdot V_i$. The process of a single-head scaled-dot product attention can be denoted as:

$$head_i = Attention(Q_i, K_i, V_i) = \operatorname{softmax}\left(\frac{Q_i \cdot K_i^{\top}}{\sqrt{D_K}}\right) \cdot V_i$$
(1)

Correspondingly, the procedure of a multi-head selfattention can be defined as:

$$M_{head} = \text{Concat}(head_1, \dots, head_m)$$
 (2)

where M_{head} refers to the output of a multi-head self-attention, Concat means the concatenation operation, m presents the head number.

2.2.3 Position-wise Feed-forward Networks

The output of each multi-head self-attention layer passes through a position-wise feed-forward network (FN) consisting of two fully-connected layers with a nonlinear activation function:

$$FN(X) = W_2 \sigma(W_1 X) \tag{3}$$

where X denotes the output of the multi-head self-attention layer, W_1 and W_2 represent the parameters of two forward linear layers respectively and σ presents the activation function, such as ReLU [45].

2.2.4 Residual Connection and Normalization

As illustrated in Figure 2a, a residual connection and normalization layer (Add&Norm) is attached after each sublayer in the encoder and decoder. The output after the residual connection and normalization can be denoted as:

$$Output_{Res} = LayerNorm(X + Sublayer(X))$$
 (4)

where LayerNorm denotes layer normalization [46] that increases the stability of gradients, X and Sublayer(X) present the input and output of a sub-layer respectively, such as the multi-head self-attention layer or position-wise feed-forward network.

2.2.5 Final layer of the decoder

The output sequence generated by the decoder is finally input to a fully-connected linear layer with a softmax layer to produce the prediction probabilities.

3 APPROACH

In this section, we present *Husformer*, an end-to-end multi-modal transformer for multi-modal human affective and cognitive state recognition that learns the fusion representation directly and efficiently from raw multi-modal data streams.

3.1 Overview

As depicted in Fig. 1, from a high-level perspective, the *Husformer* uses a position-wise fedd-forward process to fuse multi-modal signal series supplied by multiple cross-modal transformers (Section 3.4). In each cross-modal transformer, the target modality is repeatedly enhanced with low-level features from other modalities by calculating the latent cross-modal attention between the target low-level unimodal feature and the low-level fusion representation. A sequence to sequence (Seq2Seq) model, i.e., a self-attention transformer, is then utilized to process the mid-level fusion representation sequence consisting of all enhanced unimodal features and generate the adaptively weighted high-level fusion representation (Section 3.5). Specifically,

by computing multi-head self-attention (Section 2.2), the self-attention transformer analyzes the pairwise relationships across elements in the mid-level fusion representation, namely, the reinforced unimodal features, to calculate adaptive weights at different positions and so highlight critical contextual information. Finally, the high-level fusion representation is passed through fully-connected layers to make predictions (Section 3.6).

3.2 Temporal Convolutions

Let $M_1,\ M_2,\ \dots\ M_n$ denote n modalities. And let $X_{\{M_1,\dots,M_n\}}\in\mathbb{R}^{L_{M_1,\dots,M_n},D_{M_1,\dots,M_n}}$ present the raw multimodal data sequences input from these n modalities. $L_{(.)}$ and $D_{(.)}$ represent the sequence length (e.g., channel number) and dimension (e.g., sampling rate) of each unimodal input respectively in this paper. The multi-modal input sequences are passed through multiple one-dimension temporal convolution layers with different kernels to generate multiple convoluted sequences $\dot{X}_{\{M_1,\dots,M_n\}}\in\mathbb{R}^{L_{M_1,\dots,M_n},D}$ with the same dimension D:

$$\dot{X}_{\{M_1,\dots,M_n\}} = \text{Conv1D}\left(X_{\{M_1,\dots,M_n\}}, k_{\{M_1,\dots,M_n\}}\right)$$
 (5)

where, $k_{\{M_1,...,M_n\}}$ denotes the temporal convolution kernel sizes for n modalities $M_1, M_2, ... M_n$.

Each convoluted sequence aims to contain low-level local features of each modality. Furthermore, it is important that after temporal convolutions, different unimodal input sequences are projected to the same dimension, making the dot-product calculation in the following cross-modal attention module mathematically feasible.

3.3 Positional Encoding

As mentioned in the preliminary of transformer (Section 2.2), the transformer network has no awareness of positional information of the sequence, e.g., relative or absolute position of each sequence component. To introduce sufficient awareness of neighborhood elements, and thus time-related information, we follow [41] to conduct positional encoding (PE) to the convoluted sequences $\dot{X}_{\{M_1,\ldots,M_n\}}$ using sin and cos functions with different frequencies. The PE of one convoluted sequence $\dot{X} \in \mathbb{R}^{L,D}$ can be defined as a matrix as:

$$PE_{\dot{\mathbf{X}}}[pos, 2k] = \sin\left(\frac{pos}{10000^{\frac{2k}{D}}}\right)$$

$$PE_{\dot{\mathbf{X}}}[pos, 2k+1] = \cos\left(\frac{pos}{10000^{\frac{2k}{D}}}\right)$$
(6)

where $pos \in [1, ..., L]$ and $k \in [0, ..., \frac{D}{2})$.

Each characteristic dimension (i.e., column) of $PE_{\dot{X}}$ is a position index that displayed in the sinusoidal pattern. The calculated PEs $PE_{\dot{X}_{\{M_1,\ldots,M_n\}}} \in \mathbb{R}^{L_{M_1,\ldots,M_n},D}$, are then augmented with convoluted sequences $\dot{X}_{\{M_1,\ldots,M_n\}}$ to obtain the low-level temporally-aware unimodal features $Y_{M_1,\ldots,M_n} \in \mathbb{R}^{L_{M_1,\ldots,M_n},D}$:

$$Y_{\{M_1,\dots,M_n\}} = \dot{X}_{\{M_1,\dots,M_n\}} + PE_{\dot{X}_{\{M_1,\dots,M_n\}}}$$
 (7)

The extracted low-level temporally-aware unimodal features of all modalities are then concatenated to produce the low-level fusion representation $Y_F \in \mathbb{R}^{L_F,D}$:

$$Y_F = \operatorname{Concat}(Y_{M_1}, \dots, Y_{M_n}) \tag{8}$$

3.4 Cross-modal Attention Module

To provide sufficient complementary interactions and adaptions across different modalities, we respectively feed the low-level unimodal feature sequence of each modality $Y_{M_i} \in \mathbb{R}^{L_{M_i},D}$ with the low-level multi-modal fusion representation $Y_F \in \mathbb{R}^{L_F,D}$ to a cross-modal attention module that is comprised of multiple cross-modal transformer networks. Each cross-modal transformer is expected to continuously reinforce low-level unimodal features of the target modality with those of other source modalities by learning a cross-modal attention between the input unimodal sequence and the low-level fusion representation. Namely, the learned cross-modal attention inspires each target modality to directly engage in low-level unimodal features of other source modalities, which are encoded in the low-level fusion representation, to adaptively find relevant and useful information that can serve as complementary reinforcements for itself. In addition to introducing the adaptive and satisfactory awareness of correlations across multiple modalities, such a module can also help remedy noise and artifacts from the raw data by ignoring the irrelevance, e.g., interrupted features in the low-level unimodal feature sequence, when computing the cross-modal attention.

3.4.1 Cross-modal Attention

Inspired by the success of directional pairwise cross-modal attention in the multi-modal natural language processing task [39], we build up our cross-modal attention blocks. Distinct from the aforementioned work, we focus on the cross-modal attention between each individual modality and the multi-modal fusion signal, rather than between one single modality and another. This allows the model to take the coordination of more than a pair of modalities into account at the same time and reduces the potential information redundancy caused by parallel pairwise fusion. We conduct ablation study to present the benefits of our proposed cross-modal attention compared with the directional pairwise one in Section 4.6.3.

The purpose of our cross-modal attention is to learn a attention score between a target low-level unimodal feature sequence $Y_{M_i} \in \mathbb{R}^{L_{M_i},D}$ and the low-level multi-modal fusion representation $Y_F \in \mathbb{R}^{L_F,D}$, which guides the adaption and reinforcement for the target unimodal features using other source unimodal features embedded in the fusion representation. We formulate unimodal Query Q_{Uni} , fusion Key K_{Fus} and Value V_{Fus} as:

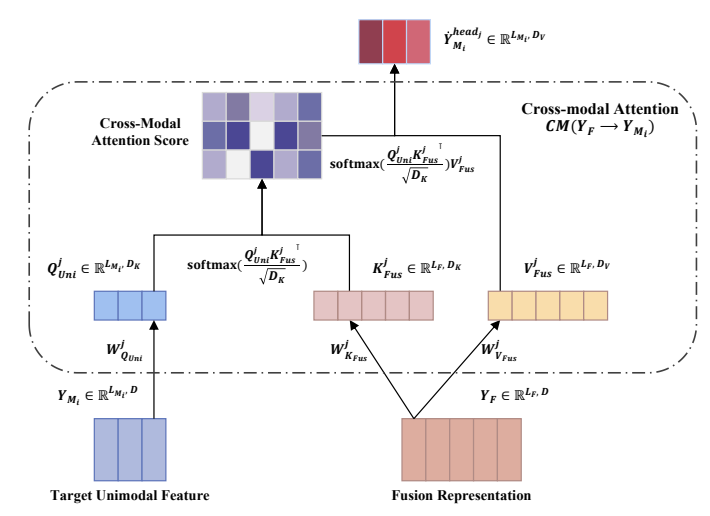
$$Q_{Uni} = Y_{M_i} \cdot W_{Q^{Uni}}$$

$$K_{Fus} = Y_F \cdot W_{K^{Fus}}$$

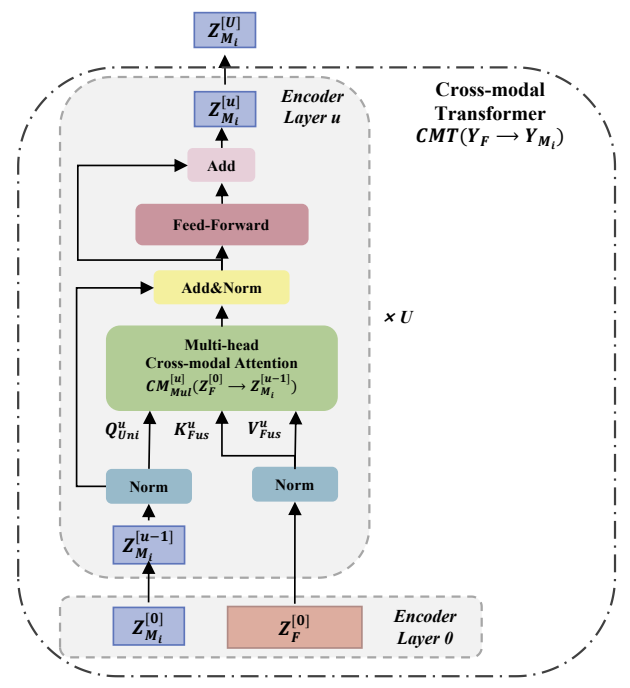
$$V_{Fus} = Y_F \cdot W_{V^{Fus}}$$
(9)

where $W_{Q^{Uni}} \in \mathbb{R}^{D,D_Q}$, $W_{K^{Fus}} \in \mathbb{R}^{D,D_K}$ and $W_{V^{Fus}} \in \mathbb{R}^{D,D_V}$ are learnable weights.

As depicted in Figure 3a, similar with the self-attention process described in Eq. (1), the latent adaption and reinforcement from the fusion representation to the target unimodal feature, i.e., the learned cross-modal attention



(a) Illustration of the cross-modal attention between each low-level unimodal feature and the low-level fusion representation.



(b) Illustration of the cross-modal Transformer network stacked by multiple identical cross-modal attention encoder layers.

Fig. 3: Architectural description of cross-modal attention and cross-modal transformer network.

 $\dot{Y}_{M_i}^{head_j} \in \mathbb{R}^{L_{M_i},D_V}$, in the j^{th} head cross-modal attention can be defined as:

$$\dot{Y}_{M_{i}}^{head_{j}} = CM(Y_{F} \to Y_{M_{i}})
= Attention(Q_{Uni}^{j}, K_{Fus}^{j}, V_{Fus}^{j})
= \operatorname{softmax} \left(\frac{Q_{Uni}^{j} \cdot K_{Fus}^{j}}{\sqrt{D_{K}}}\right) \cdot V_{Fus}^{j}$$
(10)

where the softmax(.) $\in \mathbb{R}^{L_{M_i},L_F}$ presents the scaled cross-modal attention score matrix between the fusion representation and the target unimodal feature.

We define the $\dot{Y}_{M_i}^{head_j}$ in Eq. (10) as the single-head cross-modal attention. Accordingly, the multi-head cross-modal

attention between the i^{th} target modality and the fusion representation can be formulated as:

$$\dot{Y}_{M_i}^{Mul} = CM_{Mul}(Y_F \to Y_{M_i})
= \operatorname{Concat}\left(\dot{Y}_{M_i}^{head_1}, \dots, \dot{Y}_{M_i}^{head_m}\right)$$
(11)

where $\dot{Y}_{M_i}^{Mul} \in \mathbb{R}^{L_{M_i}, mD_V}$ and m is the head number.

3.4.2 Cross-modal Transformer

Based on the structure of self-attention transformer network (see Figure 2a), we build up the cross-modal transformer using the above defined multi-head cross-modal attention. As shown in Figure 3b, the cross-modal transformer with the input of the i^{th} target unimodal feature sequence and the fusion representation, $CMT_{Y_F \to Y_{M_i}}$, is composed of multiple identical cross-modal attention encoder layers, each of which contains a multi-head cross-modal attention block and a position-wise feed-forward network with residual connection and layer normalization. Generally, a cross-modal transformer network with U cross-modal attention encoder layers calculates the reinforced unimodal feature sequence $Z_{M_i} \in \mathbb{R}^{L_{M_i},D}$ feed-forwardly as:

$$\begin{split} Z_F^{[0]} &= Y_F \\ Z_{M_i}^{[0]} &= Y_{M_i} \\ \hat{Z}_{M_i}^{[u]} &= CM_{Mul}^{[u]}(\mathbb{L}(Z_F^{[0]}) \to \mathbb{L}(Z_{M_i}^{[u-1]})) \\ \dot{Z}_{M_i}^{[u]} &= \hat{Z}_{M_i}^{[u]} + \mathbb{L}(Z_{M_i}^{[u-1]}) \\ Z_{M_i}^{[u]} &= \mathbb{F}_{\theta}(\mathbb{L}(\dot{Z}_{M_i}^{[u]})) + \mathbb{L}(\dot{Z}_{M_i}^{[u]}) \end{split} \tag{12}$$

where $u \in [1, U]$ presents the u^{th} cross-modal attention encoder layer, $\mathbb{L}(.)$ and $\mathbb{F}_{\theta}(.)$ denote the layer normalization operation and position-wise feed-forward network with a parameter set θ respectively.

In each cross-modal transformer, the target unimodal features are continuously encoded and enhanced with external information from other source unimodal features embedded in the fusion representation. Specifically, the low-level unimodal features of source modalities from the low-level fusion representation are converted to different pairs of the fusion Keys and Values in Eq. (9) to compute the multi-head cross-modal attention of the target modality in Eq. (11). Following the process described in Eq. (12), each target modality is merged with other source modalities by a position-wise feed-forward process from each cross-modal transformer.

3.5 Self-attention Module

The outputs of the cross-modal attention module, to wit the reinforced unimodal features $Z_{M_i}^{[U]} \in \mathbb{R}^{L_{M_i},D}$ of all modalities, are concatenated together as a sequence, i.e., the midlevel fusion representation $Z_{\{M_1,\dots,M_n\}} \in \mathbb{R}^{L_{M_1},\dots,M_n}$, which is transported to the self-attention transformer [41] described in Section 2.2 and demonstrated in Figure 2a to produce a weighted high-level fusion representation $Z_F \in \mathbb{R}^{L_F,D}$ with meaningful contextual information highlighted. Specifically, the self-attention transformer assigns adaptive self-attention scores to different positions in the input sequence, i.e., each minimum unit of the reinforced unimodal features of different modalities, by integrating

the global contextual information of the whole sequence. As a result, reinforced unimodal features in the sequence are given adaptive weights to generate the high-level global representation, where important contextual information for the recognition of the human state, e.g., sensitive and efficient features under a certain task scenario, is highlighted, while unimportant one, e.g., disrupted and insensitive features, is neglected. Such an adaptive self-attention process further improves the efficiency of the model and makes adjustments to noise and interruptions that still existed in the mid-level fusion representation.

3.6 Model Training

At the final step, the output of the self-attention module, namely, the high-level weighted global feature $Z_F \in \mathbb{R}^{L_F,D}$, is passed through two linear layers with a residual connection operation and a softmax nonlinear activation function that calculates prediction probabilities P as:

$$\hat{Z} = Z_F + \zeta_{\alpha}(Z_F)$$

$$P^c = \operatorname{softmax}(\zeta_{\beta}(\hat{Z}))$$
(13)

where ζ_{α} and ζ_{β} present two linear layers with parameter sets α and β , and P^c denotes the prediction probability for the c^{th} class.

Then the class with the greatest prediction probability is regarded as the predicted label:

$$\hat{y} = \arg\max_{c}(P^c) \tag{14}$$

We choose the mean-absolute error (MAE) loss function for training, which is formulated as:

$$Loss = MAE(y, \hat{y}) = -\frac{1}{N} \sum_{i=0}^{N} |y^{i} - \hat{y}^{i}|$$
 (15)

where y^i and \hat{y}^i present the $i \in [0, \dots, N]^{th}$ true label and predicted label separately.

The overall procedures of *Husformer* model training are summarized in Algorithm 1.

4 EXPERIMENT AND RESULTS

In this section, we describe our experiments conducted on the four public multi-modal human affective and cognitive state datasets, which are widely utilized in the field of human state recognition, to compare our *Husformer* with the four state-of-the-art baselines of multi-modal fusion-based human state recognition. For each dataset, the performance of using singling modality was also reported to investigate if our proposed multi-modal fusion-based *Husformer* can outperform the recognition methods using the single modality. We also conducted ablation study to evaluate the benefits of each module in the *Husformer*.

4.1 Datasets

We selected two multi-modal affective datasets: DEAP [17] and WESAD [23], and two multi-modal cognitive workload datasets: MOCAS [24] and CogLoad [25] for experiments.

The DEAP dataset contains multiple physiological signals, including EEG, EMG, EOG, and GSR, collected from

Algorithm 1 Procedures of Husformer Training

- 1: Given multi-modal data series $X_{\{M_1,\dots,M_n\}}$ of n modalities and true classification labels y
- 2: Given training steps T
- 3: Initialize convolution kernel sizes $k_{\{M_1,\dots,M_n\}}$, crossmodal attention weights $W_{Q_{Uni}},W_{K_{Fus}},W_{V_{Fus}}$, selfattention weights W_Q,W_K,W_V and other model parameters
- 4: $t \leftarrow 0$
- 5: # Convolutions and Positional Encoding
- 6: Compute low-level temporally-aware unimodal feature sequences $Y_{\{M_1,\dots,M_n\}}$ by (5)-(7)
- 7: Compute low-level fusion representation Y_F by (8)
- 8: while t < T do
- 9: # Cross-modal Attention Module
- 10: Compute reinforced unimodal feature sequences $Z_{\{M_1,\dots,M_n\}}$ by (12)
- 11: # Self-attention Module
- 12: Compute high-level fusion representation Z_F by (1)-

(4)

13:

- # Linear Layers
- 14: Compute predicted labels \hat{y} by (13)-(14)
- 15: # Model Optimization
- 16: Compute loss $MAE(y, \hat{y})$ by (15)
- 17: Update model parameters using back propagation
- 18: $t \leftarrow t + 1$
- 19: end while

32 participants watching 40 different music video clips that elicited different emotional states. After each video clip, participants were requested to report their affective state levels in terms of arousal, valence, liking, and dominance from 1 to 9 using the Self-Assessment Manikin (SAM). In our experiment, we utilized two versions of the DEAP dataset: the downloaded Data-original.zip which contained collected raw data was regarded as the raw DEAP dataset, while the downloaded Data-preprocessed.zip which preprocessed the raw data with bandpass filters and other procedures¹ was regarded as the preprocessed DEAP dataset. The details of all utilized modalities of these two versions are described in Table 2. In addition, valence and arousal were selected as the evaluation criteria of human emotion, where we mapped the scales (1-9) into three levels: "negative" or "passive" (1-3); "neutral" (4-6); and "positive" or "active" (7-9).

The WESAD dataset contains physiological data, consisting of GSR, BVP, EMG, ECG and respiration (RESP), collected by one chest-worn and one wrist-worn wearable sensor from 15 participants who conducted different tasks that aimed to elicit different emotional states. Specifically, participants were asked to close their eyes for seven minutes to stimulate the neutral state. The stress state was elicited by the Trier Social Stress Test (TSST) [47], where participants delivered a five-minute speech on their personal traits to three-person panels. Moreover, for the amusement state, participants were required to watch funny videos for 392 seconds. After each task, participants reported subjective emotional states using SAM and other self-report questionnaires, and three kinds of labels, i.e., neutral *vs.* stress *vs.*

1. https://www.eecs.qmul.ac.uk/mmv/datasets/deap/

TABLE 2: Description of utilized modalities in the DEAP. Frequency: time sampling rate; Channels: number of channels; and Array Shape: number of data rows×channels×frequency.

Raw DEAP Dataset							
Modality	Frequency	Channels	Array Shape				
EEG	512	32	69535×32×512				
EMG	512	4	$69535 \times 4 \times 512$				
EOG	512	4	$69535 \times 4 \times 512$				
GSR	512	1	$69535 \times 1 \times 512$				
	Preprocesse	d DEAP Dat	aset				
Modality	Frequency	Channels	Array Shape				
EEG	128	32	80640×32×128				
EMG	128	2	$80640 \times 2 \times 128$				
EMG EOG	128 128	2 2	$80640 \times 2 \times 128$ $80640 \times 2 \times 128$				

TABLE 3: Description of utilized modalities in the WESAD.

WESAD Dataset								
Modality	Frequency	Channels	Array Shape					
GSR (chest)	700	1	27287×1×700					
BVP (wrist)	64	1	$27287 \times 1 \times 64$					
EMG (chest)	700	1	$27287 \times 1 \times 700$					
ECG (chest)	700	1	$27287 \times 1 \times 700$					
RESP (chest)	700	1	$27287 \times 1 \times 700$					
GSR (wrist)	4	1	$27287 \times 1 \times 4$					

amusement, were provided. The details of all modalities in the WESAD dataset utilized for three-class classification are described in Table 3.

The MOCAS dataset contains physiological data, including 5-channels EEGs (i.e., AF3, AF4, T7, T8, and Pz), EEG band powers (or EEG_POW, including theta, low and high beta, alpha, and gamma bands of 5-channels EEGs), BVP, GSR and HR, and behavioral data, including Eye Aspect Ratio (EAR) and Action units (AUs), from 21 participants conducting Closed-Circuit Television (CCTV) monitoring tasks that aimed to elicit different levels of cognitive workload. After each CCTV monitoring task, participants were required to report subjective cognitive workload via NASA-TLX, and a weighted NASA-TLX score is calculated by multiplying the associated workload scales (e.g., [5, 0, 4, 3, 2, 1]) with the NASA-TLX scales. Based on the weighted NASA-TLX scores, three categories of annotations, i.e., low vs. medium vs. high, were given. Apart from the raw physiological and behavioral data collected from two off-the-shelf wearable sensors: Empatica E4 and Emotiv Insight, and a webcam, the MOCAS also contains the data prepossessed by NeuroKit2 [48] and other methods². In this experiment, we utilized both raw data and preprocessed data in the MOCAS dataset. The details of all utilized modalities of these two versions are described in Table 4.

The CogLoad dataset contains physiological signals, including HR, IBI, GSR, SKT, and motion data (ACC) collected from 23 participants through a Microsoft band. The participants conducted six dual-tasks including primary and secondary cognitive-load tasks that were expected to stimulate target levels of cognitive workload. The primary task was randomly selected from six psycho-physiological tests proposed in [49]. The secondary task was to click on the appearing target on screen while conducting the primary task. After each task, participants were asked to

2. https://polytechnic.purdue.edu/ahmrs/mocas-dataset

TABLE 4: Description of utilized modalities in the MOCAS.

Raw MOCAS Dataset							
3 5 3 34							
Modality	Frequency	Channels	Array Shape				
EEG	128	6	215341×5×128				
EEG_POW	8	25	$215341 \times 25 \times 8$				
BVP	128	1	$215341 \times 1 \times 128$				
GSR	6	1	$215341 \times 1 \times 6$				
EAR	1	1	$215341\times1\times1$				
	Preprocessed	MOCAS Da	taset				
Modality	Frequency	Channels	Array Shape				
EEG	128	6	215341×5×128				
EEG_POW	8	25	$215341 \times 25 \times 8$				
BVP	128	1	$215341 \times 1 \times 128$				
GSR	6	1	$215341 \times 1 \times 6$				
EAR	1	1	$215341 \times 1 \times 1$				

TABLE 5: Description of utilized modalities in the CogLoad.

_	CogLoad Dataset									
_N	l odality	Frequency	Channels	Array Shape						
	HR	1	1	89225×1×1						
	IBI	1	1	$89225 \times 1 \times 1$						
	GSR	1	1	$89225 \times 1 \times 1$						
	SKT	1	1	$89225 \times 1 \times 1$						
	ACC	1	2	$89225 \times 2 \times 1$						

report subjective cognitive workload based on the TLX mental demand of NASA-TLX questionnaire, and the data collected in the baseline (rest) section was labelled as -1. In our experiment, we mapped the subjective scales into three classes of labels as low (-1-3), medium (4-6) and high (7-9). Also, the details of all utilized modalities of these two versions are described in Table 5.

4.2 Baselines

We selected four state-of-the-art baselines of multi-modal fusion-based human state recognition as the comparisons with our proposed *Husformer*:

- *EF-SVM*: Support Vector Machines with early fusion [15], [18], [22]. This is a popular benchmark model for human state recognition, which concatenates different modalities together at the sensor or feature level and builds a SVM as the classifier for the fused representation.
- *LF-SVM*: Support Vector Machines with late fusion [14], [18], [22]. This model is also a strong benchmark to predict human state, which fuses different modalities at the decision level. Each modality is processed with a SVM classifier to make individual predictions, which are combined together through a voting scheme. In our experiment, we select Dempster-Shafer Theory (DST) voting [50], [51], which is reported as the best performing voting scheme by [22], as the late fusion process.
- EmotionMeter [19]. This is a multi-modal deep learning model for human emotion prediction. Multiple individual restricted Boltzmann machines (RBMs) are built to process features of each modality, where the hidden layers of those individual RBMs are concatenated together to learn the shared representations across different modalities. Then a linear SVM is adopted for classification using the learned shared representations.
- MMResLSTM: Multimodal Residual Long Short-Term Memory Neural Network [21]. This is another state-ofthe-art multi-modal deep learning model for human emo-

tion recognition. Multiple individual LSTM blocks are constructed for each modality, where each LSTM layer of these individual LSTM blocks shares the same weights to learn the temporal correlations across different modalities. Finally, the outputs of all LSTM blocks are concatenated and passed through a dense layer to make predictions. Layer normalization and residual connection are also applied to accelerate training process.

Moreover, to comprehensively evaluate if our *Husformer* could improve the performance compared with using single modality, we also implemented Long Short-Term Memory Nerual Network (LSTM) [52], Graph Neural Network (GNN) [53] and Transformer [41], which were broadly utilized for single-modal-based human state recognition [54], [55], [56], to test each single modality in each dataset, and the best performing results among these three models were reported.

4.3 Ablation Study

To evaluate the benefits of each module in our *Husformer*, we also built three ablation models for the ablation study:

- *HusFuse*: deleting the cross-modal attention module in the *Husformer*, and fusing the low-level features of all modalities directly to the self-attention module.
- *HusPair*: replacing the cross-modal attention module in the *Husformer* with the directional pairwise cross-modal attention in [39].
- *HusLSTM*: replacing the self-attention transformer in the *Husformer* with a LSTM layer.

4.4 Evaluation and Metrics

For each dataset, we randomly shuffled all data and conducted the K-folder Cross Validation (K=10) [57], [58]. We reported average multi-class average accuracy (Acc) and multi-class average F1-score (F1) [59] with standard deviations of each model in each experiment.

Assume the number of classes in a multi-class classification task is n, then the Acc can be defined as:

$$Acc = \frac{\sum_{i=1}^{n} accuracy_i}{n} \tag{16}$$

where $accuracy_i$ denotes the binary accuracy of the i^{th} class as:

$$accuracy_i = \frac{TP_i + TN_i}{lenth_i} \tag{17}$$

 TP_i , TN_i and $lenth_i$ present true positive samples, true negative samples and the number of total samples in the i^{th} class respectively.

The F1 can be formulated as:

$$F1 = \frac{\sum_{i=1}^{n} f1_i}{n}$$
 (18)

where $f1_i$ denotes the binary F1 score of the i^{th} class as:

$$f1_i = \frac{2 \times precision_i \times recall_i}{precision_i + recall_i}$$
 (19)

$$precision_i = \frac{TP_i}{TP_i + FP_i} \tag{20}$$

$$recall_i = \frac{TP_i}{TP_i + FN_i} \tag{21}$$

where $precision_i$ and $recall_i$ present the binary precision and recall separately, FP_i and FN_i denote false positive and false negative samples in the i^{th} class respectively.

We also conducted two-sample independent t-tests to compare the classification results of different models, and the significance is asserted when p < 0.01.

4.5 Implementation Details

All training and experiments were conducted on a NVIDIA Tesla V100 GPU. We trained all baseline networks by following the implementing procedures described in the original papers. Also, for the SVM classifier, we follow [22] to select the Radial Basis Function (RBF) kernel and optimize the C and gamma values. Note that EF-SVM cannot be directly applied to unaligned datasets, namely, datasets that contain multiple modalities with different time sampling rates, since different feature dimension makes the concatenation operation mathematically impossible. Therefore, we added multiple one-dimension convolution sub-networks with the same structures and parameters as those in the Husformer before the *EF-SVM* to extract low-level unimodal features with the same dimension for the concatenation operation on unaligned datasets, i.e., WESAD and MOCAS datasets. Furthermore, for a fair comparison, the hyper-parameters of ablation models were kept the same as the *Husformer* during the experiments. The hyper-parameters of the Husformer in each experiment could be found in Appendix A.³

4.6 Quantitative Measurements

4.6.1 Comparative Results with Baselines

Table 6 and 7 summarize the performance of our *Husformer* when compared with the four multi-modal baselines of human state recognition in terms of average Acc and F1with stand deviations during the experiments. From the comparative results, we can observe that regarding the overall performance, our proposed Husformer outperforms other four state-of-the-art baselines in the recognition of both human affective state (DEAP and WESAD datasets) and cognitive workload (MOCAS and CogLoad datasets), which demonstrates that the *Husformer* can serve as a more effective backbone network for general human state prediction tasks. Also, such performance enhancements are more evident on datasets containing multi-modal raw data (raw DEAP and MOCAS, WESAD and CogLoad datasets), which shows that the Husformer can learn from multi-modal raw data series more efficiently, and thus is more applicable to real-world task scenarios where extensive data preprocessing is quite impractical and expensive. These performance improvements mainly result from following reasons:

• Experimental results show that our *Husformer* significantly outperforms *EF-SVM* and *LF-SVM* regarding *Acc* and *F*1 on each dataset. This is reasonable since these two methods generate fusion representations by a simple concatenation of multiple modalities at the feature or decision level, which ignores correlations across different

3. Source code for our *Husformer* and experiments are available at: https://github.com/SMARTlab-Purdue/Husformer.

TABLE 6: Performance of different models on raw DEAP and prepossessed DEAP datasets in terms of average multi-class average accuracy (Acc) and multi-class average F1-score (F1) with stand deviations. Results of other models that are within 5% of the Husformer's on Acc or F1 are highlighted. h: higher is better; h: results obtained from [21]; and h: not reported.

Dataset		Raw l	DEAP		Preprocessed DEAP				
Criteria	Vale	ence	Aro	Arousal		Valence		Arousal	
Metric	$Acc(\%)^h$	$F1(\%)^{h}$	$Acc(\%)^h$	$F1(\%)^h$	$Acc(\%)^h$	$F1(\%)^h$	$Acc(\%)^h$	$F1(\%)^{h}$	
EF-SVM	48.16±2.04	51.57 ± 2.40	50.23±1.97	52.90±2.03	74.89±6.17	76.61 ± 6.39	75.25 ± 5.84	75.39 ± 6.01	
LF-SVM	51.02±4.63	55.83 ± 4.99	54.11 ± 3.82	57.33 ± 3.77	73.52 ± 5.41	75.30 ± 5.58	76.17 ± 4.76	77.04 ± 4.90	
EmotionMeter	67.94±3.24	68.23 ± 3.18	68.31 ± 2.95	68.41 ± 2.87	85.49 ± 2.31	85.82 ± 2.49	86.25 ± 3.11	86.41 ± 3.04	
MMResLSTM	72.41±1.87	73.12 ± 1.79	73.04 ± 1.52	73.12 ± 1.60	$93.51{\pm}2.30$	93.76 ± 2.29	93.28 ± 1.52	$93.86{\pm}1.99$	
MMResLSTM♦		_	_	_	92.30±1.55	_	$92.87{\pm}2.11$	_	
HusFuse	73.26±3.04	74.45 ± 2.97	73.66 ± 2.48	73.89 ± 2.34	86.29±1.39	86.58±1.52	87.07±1.19	87.23±1.29	
HusPair	83.26±2.25	$82.83{\pm}2.18$	$83.67{\pm}2.07$	$83.17{\pm}1.94$	$95.54{\pm}3.18$	$95.38{\pm}2.84$	$96.43{\pm}2.84$	$96.27{\pm}2.91$	
HusLSTM	78.42±2.12	$78.85{\pm}2.15$	76.79 ± 1.68	77.16 ± 1.71	89.17±1.68	89.97 ± 1.87	90.37 ± 1.36	90.49 ± 1.25	
HusFormer	85.98±1.38	86.21±1.40	$86.28{\pm}2.04$	86.78 ± 2.11	97.01±2.06	97.08±2.15	$97.67{\pm}1.45$	97.69±1.53	

TABLE 7: Performance of different models on WESAD, raw MOCAS, preprocessed MOCAS and CogLoad datasets in terms of average multi-class average accuracy (Acc) and multi-class average F1-score (F1) with stand deviations. Results of other models that are within 5% of the Husformer's on Acc or F1 are highlighted. h: higher is better.

Dataset	WESAD		Raw MOCAS		Preprocessed MOCAS		CogLoad	
Metric	$Acc(\%)^h$	$F1(\%)^h$	$Acc(\%)^h$	$F1(\%)^{h}$	$Acc(\%)^h$	$F1(\%)^h$	$Acc(\%)^h$	$F1(\%)^h$
EF-SVM	46.67±4.21	48.60±3.95	55.69±4.26	55.84±4.87	66.94±4.78	66.08±4.06	45.88±3.67	51.73±3.01
LF-SVM	49.19 ± 2.35	51.72 ± 2.87	52.95 ± 3.27	53.06 ± 3.29	64.01±5.03	64.89 ± 4.94	43.19 ± 2.58	50.08 ± 1.99
EmotionMeter	69.24±1.20	69.44 ± 1.13	77.38 ± 3.27	77.21 ± 3.18	85.03±2.33	86.17 ± 2.40	65.80 ± 1.21	69.22 ± 1.09
MMResLSTM	72.49 ± 0.86	73.05 ± 0.98	82.06±2.15	82.17±1.95	89.54±1.08	89.98±1.14	68.17±1.41	70.12 ± 1.45
HusFuse	74.58±1.37	74.29 ± 1.12	76.46±2.17	77.03±2.20	83.81±1.91	84.62±1.67	64.30±0.49	63.46 ± 0.64
HusPair	80.69 ± 1.57	79.89 ± 1.98	88.24 ± 1.68	88.58 ± 1.48	$94.95{\pm}3.82$	$94.87{\pm}3.84$	71.23 ± 2.92	72.67 ± 3.10
HusLSTM	76.40 ± 0.99	76.76 ± 1.06	84.74±2.50	85.04±2.39	88.16±1.58	88.30 ± 1.56	72.85 ± 0.84	72.36 ± 0.79
HusFormer	85.02±1.91	85.85±2.14	93.71±2.26	$93.82{\pm}2.41$	96.42±2.11	96.51±2.03	80.40±2.34	$81.27{\pm}2.63$

modalities, and may be limited by the curse of dimensionality [31], while the Husformer fuses all unimodal features through a feed-forward process from multiple crossmodal attention transformers, where the complementary interactions among different modalities are considered sufficiently. Such a neglect of cross-modal interactions even makes the performance of the *EF-SVM* and *LF-SVM* be exceeded by the *EmotionMeter* and *MMResLSTM* by about 10% on Acc and F1. These comparative results highlight the significance of awareness of correlations across multiple modalities for multi-modal human state recognition. Moreover, the SVM, which serves as the backbone model in the *EF-SVM* and *LF-SVM*, has been proved to usually have low efficiency when facing a large amount of data input [60] and is quite sensitive to missing data, outliers and noise [61]. As a result, it depends heavily on careful data cleaning and feature selection procedures to be reasonable. Thus, while some studies demonstrate that EF-SVM and LF-SVM are sufficient to estimate human state with a high volume of data cleaning and careful feature crafting [21], [22], it is sensible that EF-SVM and LF-SVM perform badly when dealing with raw multimodal signals.

• Experimental outcomes present that our *Husformer* significantly outperforms *EmotionMeter* regarding *Acc* and *F*1 on all datasets. We argue that the reason lies in that although it considers cross-modal interactions by building shared hidden layers to learn shared representations, the constructed RBMs neglect time-related cross-modal interactions, which are very important as the temporal characteristic is a critical attribute of signals reflecting human state [5], [21]. *MMResLSTM*, on the other hand,

achieves better performance than EmotionMeter and are even competitive to our *Husformer* on the preprocessed DEAP and preprocessed MOCAS datasets. This is due to that MMResLSTM constructs LSTM layers that share the same weights for different modalities to learn shared representations, which clearly model the temporal crossmodal correlations. However, on the other four datasets without any data preprocessing, the Husformer still significantly outperforms the MMResLSTM regarding Acc and F1. We argue that the reason lies in that distinct from sharing the same weights among LSTM sub-layers of each modality, our proposed cross-modal attention mechanism considers cross-modal interactions by encouraging one modality to directly engage in the unimodal features of other modalities where strongly complementary representation information is presented to enhance itself. Such an attention-based fusion strategy can capture complicated and long-term complementary interactions across multiple modalities more efficiently, especially when dealing with multi-modal raw data that is filled with noise and interruptions.

• The performance augmentations of our *Husformer* beyond the other four baselines are more obvious when shifting from preprocessed datasets to raw datasets. This is reasonable due to the cross-modal attention and self-attention modules utilized in the *Husformer*. Specifically, in addition to modeling the complicated complementary multi-modal interactions from raw multi-modal signals efficiently, the cross-modal transformers can adjust the noise and artifacts in the raw data through neglecting irrelevance, e.g., interrupted low-level unimodal features, when calculating an adaptive cross-modal attention. Moreover, the self-

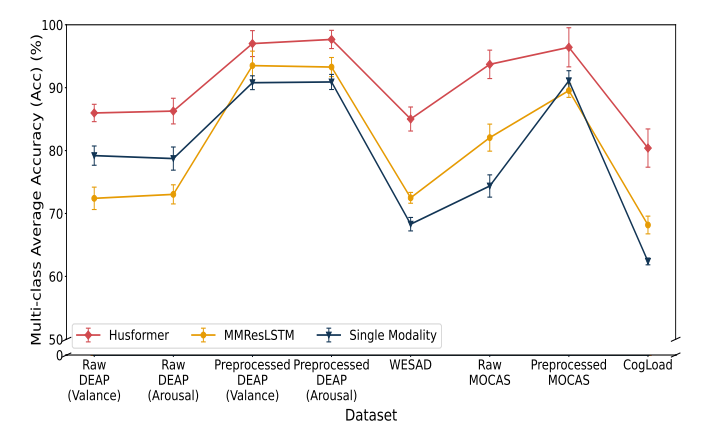


Fig. 4: Performance of *Husformer* and *MMResLSTM* when compared to the best performing result utilizing single modality on each dataset in terms of multi-class average accuracy.

attention process further prioritizes the important information and diminishes the interruptions by giving adaptive weights to each element in the sequence consisting of reinforced unimodal features of different modalities. Compared with all baselines, such two adaptive attention mechanisms at the fusion process and high-level feature level respectively can help the model to distill effectual representations of human state without being disturbed by the noise in the multi-modal raw data to a greater extent.

4.6.2 Comparative Results with Single Modality

Figure 4 summarizes the performance of our *Husformer* and the best performing multi-modal fusion baseline MM-ResLSTM when compared with the best performing recognition result of utilizing a single modality on each dataset in terms of Acc. The details of the classification results using each single modality in each dataset with regard to both Acc and F1 are reported in Appendix B. As shown in Figure 4, our proposed Husformer significantly outperforms the best performing single-modal-based recognition results on all four datasets in terms of Acc. We assume that such improvements result from the fact that our Husformer can effectively leverage the aforementioned advantages of multi-modal fusion for human state recognition, such as combing metrics from different sources to unveil essential representation information that cannot be obtained from one single source [9] and reducing the noise-to-signal ratio [5]. Meanwhile, we can observe that the MMResLSTM, another multi-modal fusion-based model which achieves the best performance among all baselines, does not outperform the single EEG related modality-based recognition with transformer networks on the raw DEAP and preprocessed MOCAS datasets. This demonstrates that the cross-modal attention and self-attention processes introduced enable the Husformer to take more advantages of the multi-modal fusion by modeling sufficient and long-term complementary cross-modal correlations and adaptively highlighting meaningful contextual representations.

4.6.3 Results of the Ablation Study

Table 6 and 7 present the performance of the *Husformer* in terms of *Acc* and *F*1 on each dataset when compared to three ablation models, the *HusFuse*, *HusPair*, and *HusLSTM*. From the results, we can observe the effectiveness of the cross-modal and self-attention module inside the *Husformer* as followings:

Effectiveness of the cross-modal attention module

- Compared with the HusFuse which removes the crossmodal attention module in the Husformer, the Husformer achieves an absolute improvement of $11.39\% \sim 18.04\%$ on Acc and $10.34\% \sim 18.37\%$ on F1. We believe the reason lies in that the HusFuse fuses low-level features from different modalities together with a simple concatenation operation instead of a feed-forward process from cross-modal transformers. While the following selfattention processes in the *HusFuse*, that relates entities of the sequence concatenated by low-level features from different modalities with contextual information to calculate the high-level fusion representation, can be regarded as a consideration of cross-modal interactions in a way, it fails to provide the direct complementary adaptions for features of one modality with those of the other modalities during the fusion process. This result verifies the effectiveness of the fusion strategy of the proposed cross-modal attention compared to simple concatenations with the self-attention.
- Compared with the HusPair that replaces the cross-modal attention module in the Husformer with the directional pair-wise cross-modal attention in [39], the Husformer achieves an improvement of $1.24\% \sim 10.35\%$ on Acc and $1.42\% \sim 11.29\%$ on F1. We argue that this is because the pairwise cross-modal attention in the HusPair can only consider the complementary adaptions between a pair of modalities at once and thus ignores the coordination among more than two modalities. In contrast, our proposed cross-modal attention computes the complementary interactions between the low-level unimodal features of one target modality and the low-level fusion representation embedded with unimodal features of the other source modalities. This allows the model to take the coordination across all modalities at the same time, hence, considers more long-term and comprehensive cross-modal interactions. Moreover, it has been shown that the pairwise fusion approach can produce redundant fusion information that may serve as the additional noise rather than effectual multi-modal features [62], [63].

TABLE 8: The number of parameters and GPU memory usage during the training of the *Husformer* and *Huspair* on each dataset. Para: the number of parameters; Mem: GPU memory usage.

Dataset	Rav	w DEAP	Preproc	essed DEAP	W	/ESAD	Raw	MOCAS	Preproce	essed MOCAS	Co	gload
Metric	Para	Mem	Para	Mem	Para	Mem	Para	Mem	Para	Mem	Para	Mem
HusPair	2.90M	3253.24MB	2.92M	2908.66MB	3.90M	5416.90MB	6.21M	519.67MB	6.22M	531.80MB	3.12M	202.47MB
Husformer	0.63M	1999.56MB	0.66M	1773.59MB	0.71M	3084.35MB	0.74M	210.97MB	0.75M	220.53MB	0.72M	94.28MB

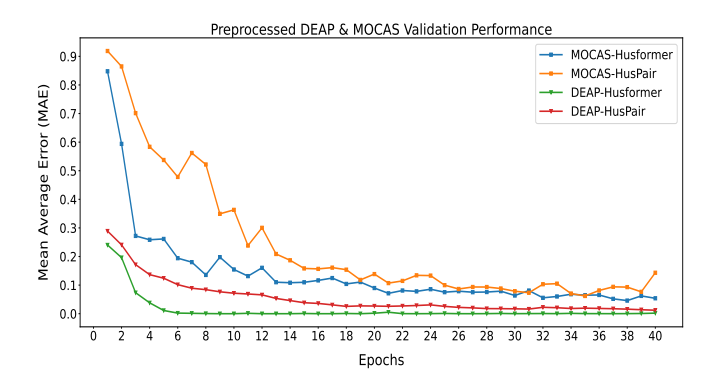


Fig. 5: Learning curves of Husformer when compared to Hus-Pair on the preprocessed DEAP and MOCAS datasets in terms of validation set convergence.

only requires 6 of them. Such a high volume of parameters can result in a slow convergence and high training difficulty. For example, on the preprocessed DEAP and the preprocessed MOCAS where the *HusPair* gets its most competitive results, we empirically observe that the Husformer can converge faster to a lower loss compared to the HusPair during the training process (see Figure 5). Furthermore, we also assume that such pairwise cross-modal attention with potential over-parameterization issues may also produce attention redundancy when the feature complexity cannot meet that of the attention, e.g., regarding the noise or artifacts as a part of the learned attention. For example, on the CogLoad dataset where the feature length (channel number) and dimension (sampling frequency) are very shallow compared to those in other datasets, the performance of the *HusPair* drops significantly, exceeded by the *Husformer* by 10% (see Table 6 and 7). Therefore, the expensive storage and computation costs (see Table 8), and the possible ineffectiveness on the shallow modalities resulting from the huge amount of parameters diminish the applicability of the HusPair to general and practical task scenarios of multi-modal human state recognition. On the contrary, our *Husformer* can achieve comparable and even significantly superior performance with much fewer parameters than the HusPair. These results highlight the effectiveness of our proposed cross-modal attention compared with the directional pairwise one.

Effectiveness of the self-attention module

• Compared with the *HusLSTM* that replaces the self-attention module in the *Husformer* with a LSTM layer, the *Husformer* achieves an absolute improvement of $7.30\% \sim 9.49\%$ on Acc and $7.11\% \sim 9.62\%$ on F1. We believe that such an improvement results from that the self-attention mechanism applied in the transformer network [41], which enables the model to capture long-term tempo-

ral dependencies by considering the sequence consisting of all reinforced unimodal features as a whole. In contrast, the LSTM processes the sequence element by element, which can suffer from long-dependency issues [64]. Moreover, the self-attention mechanism can adaptively highlight meaningful contextual information while reducing useless one by computing adaptive attention scores at a different position in the sequence, leading to a more effectual global representation of human state. This result proves the effectiveness of the self-attention module in the *Husformer*.

4.7 Qualitative Analysis

To demonstrate how the cross-modal attention and selfattention in the Husformer work when learning from multimodal signals of human state, we visualize the attention activation for qualitative analysis. Figure 6 shows an example cross-modal attention weight group consisting of learned cross-modal attention matrices at the final layer of each cross-modal transformer within 3 batches during the training on the raw MOCAS dataset. Note that the original cross-modal attention score matrix between a target low-level unimodal feature sequence and the low-level fusion representation on one batch has the dimension of $L_{M_i} \times L_F$ (see Figure 3a). We can observe that the crossmodal attention has learned how to attend to positions revealing relevant and meaningful information across the target modality and source modalities embedded in the fusion representation. For instance, higher cross-modal attention scores are assigned to some intersections of the BVP and GSR unimodal features and part of the EEG_POW unimodal features embedded in the later part (8-32) of the fusion representation.

Furthermore, we can notice that the learned cross-modal attention is adaptive; i.e., different cross-modal attention patterns are learned between different target modalities and the fusion representation. Such patterns even have some differences for the same target modality across different patches. For instance, while the EEG modality is always encouraged to attend to the later section (8-32) of the fusion representation, i.e., the EEG_POW modality, the intersections assigned with higher cross-modal attention scores vary from different batches. On the other hand, despite of the above adaptive differences, we can notice that some stable and consistent cross-modal attention patterns exist in different batches of the same target modality. For example, higher cross-modal attention scores are always assigned to the intersections of the EEG POW unimodal features and the BVP, GSR and EEG unimodal features embedded in the front positions (1-7) in the fusion representation. These observations over the visualized cross-modal attention score matrices demonstrate that our proposed cross-modal attention module can capture and model an adaptive but

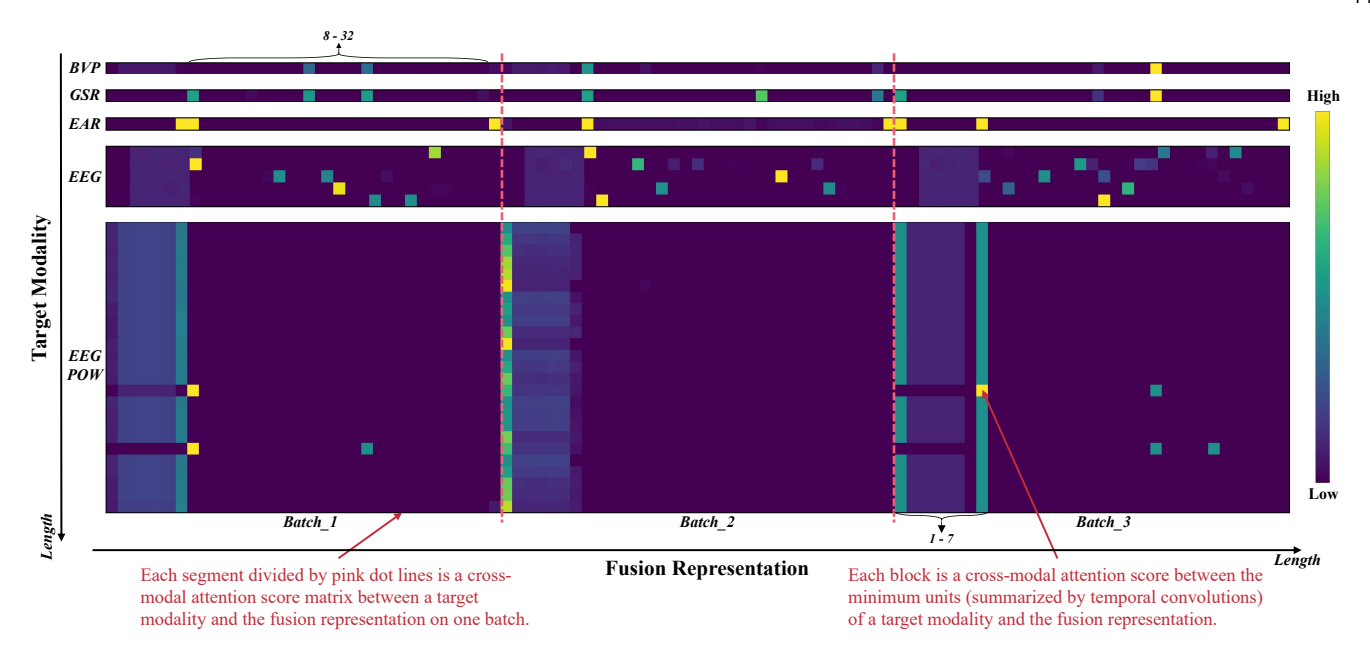


Fig. 6: Visualization of an example cross-modal attention weight group consisting of learned cross-modal attention matrices at the final layer of each cross-modal transformer within 3 batches during the training on the raw MOCAS dataset. Note that the cross-modal attention score matrix between a target low-level unimodal feature and the low-level fusion representation on one batch has the dimension of $L_{M_i} \times L_F$, i.e., the length of the target unimodal feature plus that of the fusion representation (BVP, GSR and EAR: 1×33 ; EEG: 5×33 ; EEG_POW: 25×33).

relatively consistent and long-term pattern of cross-modal interactions.

Figure 7a depicts an example of the output of the selfattention transformer in the Husformer, namely the highlevel fusion representation $Z_F \in \mathbb{R}^{L_F,D}$, within 3 batches during the training on the raw MOCAS dataset. We can observe that the self-attention has learned how to prioritize important contextual information for human state recognition and reduce the insignificant one by assigning high (blue) and low (red) self-attention scores to different positions in the fusion representation. Also, similar to the cross-modal attention, the learned self-attention is adaptive; i.e., different minimum units in the fusion representation are assigned with self-attention scores in different patterns, especially from the 'Dimension' axis. Meanwhile, we can notice that the learned self-attention patterns of the features of the same modality share many similarities across different batches, especially for EEG and EEG_POW modalities. These observations demonstrate that the self-attention in the Husformer can highlight the effectual contextual features of human state and diminishes ineffectual ones in the fusion representation with an adaptive while relatively steady pattern.

Meanwhile, Figure 7b depicts an example of the high-level fusion representation output of the self-attention transformer in the *HusFuse*. Note that the inputs of the self-attention transformers in the *Husformer* and *HusFuse* are concatenated by unimodal features of each modality within the same fragments. The only difference is that the unimodal features in the input of the *Husformer*'s are reinforced by cross-modal attention transformers while those in the *HusFuse*'s are not. Comparing the different self-attention patterns assigned to the same fragments of unimodal features in the fusion representation as illustrated in Figure

7a and 7b, we can notice that without the cross-modal attention modelling the cross-modal interactions, the self-attention learned in the *HusFuse* is less efficient; that is, only few of high (blue) and low (red) self-attention scores are assigned to features in the fusion representation, leading to insufficient prominence of critical contextual information and diminishing of unimportant one respectively. We can also notice that the self-attention is less consistent; that is, no stable self-attention patterns are shown on features of the same modality across batches, especially between the *Batch_1* and *Batch_3*. Such differences demonstrate that the reinforcements for unimodal features from the cross-modal attention in the *Husformer* can help the self-attention highlight critical contextual information in the fusion representation with a more efficient and consistent pattern.

5 CONCLUSION AND FUTURE WORK

In this paper, we propose Husformer, an end-to-end multimodal transformer framework for the recognition of multimodal human state, including human affective state and cognitive workload. In modelling multi-modal features, Husformer fuses modalities with adaptive and sufficient cross-modal interactions, inspiring one modality to directly attend to features of other modalities where strong crossmodal relevance exists. In addition, Husformer can adaptively highlight important contextual information in the fusion representation. Experimental results on four public benchmark multi-modal datasets of human emotion and cognitive workload demonstrated the effectiveness of the proposed Husformer on the general human state recognition; specifically, it outperformed four other state-of-the-art multi-modal-based baselines and demonstrated enhanced performance over using a single modality. Additionally,

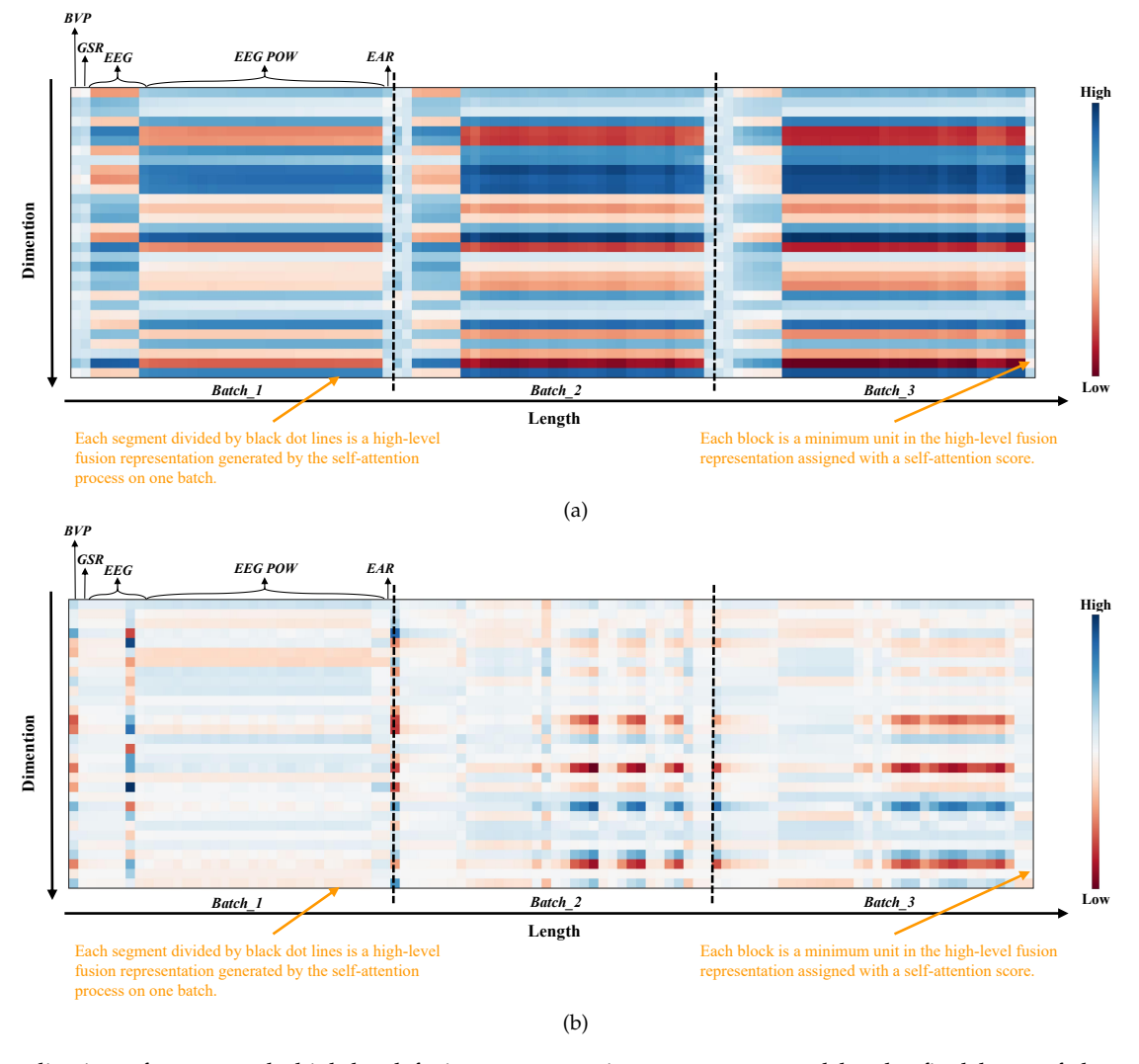


Fig. 7: Visualization of an example high-level fusion representation group generated by the final layer of the self-attention transformer in the (a) HusFormer and (b) HusFuse within 3 batches during the training on the raw MOCAS dataset. Note that the high-level fusion representation produced on one batch has the dimension of $L_F \times D$, i.e., 33×30 .

the ablation study highlighted the effectiveness of two key components in the *Husformer*, the cross-modal attention and self-attention modules. Through visualization of attention activation, we demonstrated that the cross-modal attention and self-attention transformers introduced in *Husformer* can respectively model adaptive but relatively consistent and long-term cross-modal interactions of multiple modalities and contextual interactions in the high-level fusion representation.

While we argue and demonstrate that *Husformer* has promising potential for realistic task scenarios of human state recognition, we only tested and proved its performance on datasets collected statically in the lab. Therefore, in the future, we plan to verify *Husformer* in and adapt it to realworld and real-time task scenarios. Furthermore, we will integrate consideration of user sensitivity into the framework to improve its performance and generalization ability.

ACKNOWLEDGEMENTS

This material is based upon work supported by the National Science Foundation under Grant No. IIS-1846221. Any

opinions, findings, and conclusions or recommendations expressed in this material are those of the author(s) and do not necessarily reflect the views of the National Science Foundation.

REFERENCES

- [1] J. Zhang, Z. Yin, and R. Wang, "Recognition of mental workload levels under complex human–machine collaboration by using physiological features and adaptive support vector machines," *IEEE Transactions on Human-Machine Systems*, vol. 45, no. 2, pp. 200–214, 2014.
- [2] C. D. Wickens, "Multiple resources and performance prediction," Theoretical issues in ergonomics science, vol. 3, no. 2, pp. 159–177, 2002.
- [3] S. Yang, Z. Yin, Y. Wang, W. Zhang, Y. Wang, and J. Zhang, "Assessing cognitive mental workload via eeg signals and an ensemble deep learning classifier based on denoising autoencoders," Computers in biology and medicine, vol. 109, pp. 159–170, 2019.
- [4] S. P. Marshall, "The index of cognitive activity: Measuring cognitive workload," in *Proceedings of the IEEE 7th conference on Human Factors and Power Plants*. IEEE, 2002, pp. 7–7.
- [5] E. Debie, R. F. Rojas, J. Fidock, M. Barlow, K. Kasmarik, S. Anavatti, M. Garratt, and H. A. Abbass, "Multimodal fusion for objective assessment of cognitive workload: a review," *IEEE transactions on cybernetics*, vol. 51, no. 3, pp. 1542–1555, 2019.

- [6] N. Sebe, I. Cohen, and T. S. Huang, "Multimodal emotion recognition," in *Handbook of pattern recognition and computer vision*. World Scientific, 2005, pp. 387–409.
- [7] Z. He, Z. Li, F. Yang, L. Wang, J. Li, C. Zhou, and J. Pan, "Advances in multimodal emotion recognition based on braincomputer interfaces," *Brain sciences*, vol. 10, no. 10, p. 687, 2020.
- [8] R. R. Brooks and S. S. Iyengar, Multi-sensor fusion: fundamentals and applications with software. Prentice-Hall, Inc., 1998.
- [9] D. Lahat, T. Adali, and C. Jutten, "Multimodal data fusion: an overview of methods, challenges, and prospects," *Proceedings of* the IEEE, vol. 103, no. 9, pp. 1449–1477, 2015.
- [10] F. Chen, J. Zhou, Y. Wang, K. Yu, S. Z. Arshad, A. Khawaji, and D. Conway, Robust multimodal cognitive load measurement. Springer, 2016.
- [11] J.-L. Kruger, S. Doherty, W. Fox, and P. De Lissa, "Multimodal measurement of cognitive load during subtitle processing," *Innovation and expansion in translation process research*, vol. 267, 2018.
- [12] Y. Huang, J. Yang, P. Liao, and J. Pan, "Fusion of facial expressions and eeg for multimodal emotion recognition," Computational intelligence and neuroscience, vol. 2017, 2017.
- [13] H. Tang, W. Liu, W.-L. Zheng, and B.-L. Lu, "Multimodal emotion recognition using deep neural networks," in *International Confer*ence on Neural Information Processing. Springer, 2017, pp. 811–819.
- [14] F. Putze, J.-P. Jarvis, and T. Schultz, "Multimodal recognition of cognitive workload for multitasking in the car," in 2010 20th International Conference on Pattern Recognition. IEEE, 2010, pp. 3748–3751.
- [15] M. A. Hogervorst, A.-M. Brouwer, and J. B. Van Erp, "Combining and comparing eeg, peripheral physiology and eye-related measures for the assessment of mental workload," Frontiers in neuroscience, vol. 8, p. 322, 2014.
- [16] "Seed dataset." [Online]. Available: https://bcmi.sjtu.edu.cn/home/seed/seed.html
- [17] S. Koelstra, C. Muhl, M. Soleymani, J.-S. Lee, A. Yazdani, T. Ebrahimi, T. Pun, A. Nijholt, and I. Patras, "Deap: A database for emotion analysis; using physiological signals," *IEEE transactions* on affective computing, vol. 3, no. 1, pp. 18–31, 2011.
- [18] P. Zhang, X. Wang, J. Chen, and W. You, "Feature weight driven interactive mutual information modeling for heterogeneous biosignal fusion to estimate mental workload," Sensors, vol. 17, no. 10, p. 2315, 2017.
- [19] W.-L. Zheng, W. Liu, Y. Lu, B.-L. Lu, and A. Cichocki, "Emotionmeter: A multimodal framework for recognizing human emotions," *IEEE transactions on cybernetics*, vol. 49, no. 3, pp. 1110–1122, 2018.
- [20] J.-L. Qiu, W. Liu, and B.-L. Lu, "Multi-view emotion recognition using deep canonical correlation analysis," in *International Confer*ence on Neural Information Processing. Springer, 2018, pp. 221–231.
- [21] J. Ma, H. Tang, W.-L. Zheng, and B.-L. Lu, "Emotion recognition using multimodal residual lstm network," in *Proceedings of the 27th ACM international conference on multimedia*, 2019, pp. 176–183.
- [22] T. Zhou, J. S. Cha, G. Gonzalez, J. P. Wachs, C. P. Sundaram, and D. Yu, "Multimodal physiological signals for workload prediction in robot-assisted surgery," ACM Transactions on Human-Robot Interaction (THRI), vol. 9, no. 2, pp. 1–26, 2020.
- [23] P. Schmidt, A. Reiss, R. Duerichen, C. Marberger, and K. Van Laerhoven, "Introducing wesad, a multimodal dataset for wearable stress and affect detection," in *Proceedings of the 20th ACM international conference on multimodal interaction*, 2018, pp. 400–408.
- [24] W. Jo, R. Wang, S. Sun, R. K. Senthilkumaran, D. Foti, and B.-C. Min, "MOCAS: A Multimodal Dataset for Objective Cognitive Workload Assessment on Simultaneous Tasks," Aug. 2022. [Online]. Available: https://doi.org/10.5281/zenodo.7023242
- [25] M. Gjoreski, T. Kolenik, T. Knez, M. Luštrek, M. Gams, H. Gjoreski, and V. Pejović, "Datasets for cognitive load inference using wearable sensors and psychological traits," *Applied Sciences*, vol. 10, no. 11, p. 3843, 2020.
- [26] J. Ngiam, A. Khosla, M. Kim, J. Nam, H. Lee, and A. Y. Ng, "Multimodal deep learning," in ICML, 2011.
- [27] D. A. Belsley, E. Kuh, and R. E. Welsch, Regression diagnostics: Identifying influential data and sources of collinearity. John Wiley & Sons, 2005.
- [28] F. Chen, N. Ruiz, E. Choi, J. Epps, M. A. Khawaja, R. Taib, B. Yin, and Y. Wang, "Multimodal behavior and interaction as indicators of cognitive load," ACM Transactions on Interactive Intelligent Systems (TiiS), vol. 2, no. 4, pp. 1–36, 2013.

- [29] Z. Wei, D. Zhuang, X. Wanyan, H. Zhang, and C. Liu, "A theoretical model of mental workload in pilots based on multiple experimental measurements," in *International Conference on Engineering Psychology and Cognitive Ergonomics*. Springer, 2014, pp. 104–113.
- [30] Y. Guo, D. Freer, F. Deligianni, and G.-Z. Yang, "Eye-tracking for performance evaluation and workload estimation in space telerobotic training," *IEEE Transactions on Human-Machine Systems*, vol. 52, no. 1, pp. 1–11, 2021.
- [31] C.-H. Wu, J.-C. Lin, and W.-L. Wei, "Survey on audiovisual emotion recognition: databases, features, and data fusion strategies," APSIPA transactions on signal and information processing, vol. 3, 2014.
- [32] A. Prakash, K. Chitta, and A. Geiger, "Multi-modal fusion transformer for end-to-end autonomous driving," in *Proceedings of the IEEE/CVF Conference on Computer Vision and Pattern Recognition*, 2021, pp. 7077–7087.
- [33] S. Wu, S. Bondugula, F. Luisier, X. Zhuang, and P. Natarajan, "Zero-shot event detection using multi-modal fusion of weakly supervised concepts," in *Proceedings of the IEEE Conference on Computer Vision and Pattern Recognition*, 2014, pp. 2665–2672.
- [34] H. Zhu, J.-B. Weibel, and S. Lu, "Discriminative multi-modal feature fusion for rgbd indoor scene recognition," in *Proceedings* of the IEEE Conference on Computer Vision and Pattern Recognition, 2016, pp. 2969–2976.
- [35] J. Kalajdjieski, E. Zdravevski, R. Corizzo, P. Lameski, S. Kalajdziski, I. M. Pires, N. M. Garcia, and V. Trajkovik, "Air pollution prediction with multi-modal data and deep neural networks," *Remote Sensing*, vol. 12, no. 24, p. 4142, 2020.
- [36] J. Zhou, K. Yu, F. Chen, Y. Wang, and S. Z. Arshad, "Multimodal behavioral and physiological signals as indicators of cognitive load," in The Handbook of Multimodal-Multisensor Interfaces: Signal Processing, Architectures, and Detection of Emotion and Cognition-Volume 2, 2018, pp. 287–329.
- [37] F. Putze, J.-P. Jarvis, and T. Schultz, "Multimodal recognition of cognitive workload for multitasking in the car," in 2010 20th International Conference on Pattern Recognition, 2010, pp. 3748–3751.
- [38] S. Barua, M. U. Ahmed, and S. Begum, "Towards intelligent data analytics: A case study in driver cognitive load classification," *Brain sciences*, vol. 10, no. 8, p. 526, 2020.
- [39] Y.-H. H. Tsai, S. Bai, P. P. Liang, J. Z. Kolter, L.-P. Morency, and R. Salakhutdinov, "Multimodal transformer for unaligned multimodal language sequences," in *Proceedings of the conference*. Association for Computational Linguistics. Meeting, vol. 2019. NIH Public Access, 2019, p. 6558.
- [40] G. Andrew, R. Arora, J. Bilmes, and K. Livescu, "Deep canonical correlation analysis," in *International conference on machine learning*. PMLR, 2013, pp. 1247–1255.
- [41] A. Vaswani, N. Shazeer, N. Parmar, J. Uszkoreit, L. Jones, A. N. Gomez, Ł. Kaiser, and I. Polosukhin, "Attention is all you need," Advances in neural information processing systems, vol. 30, 2017.
- [42] V. Shiv and C. Quirk, "Novel positional encodings to enable tree-based transformers," Advances in Neural Information Processing Systems, vol. 32, 2019.
- [43] G. Ke, D. He, and T.-Y. Liu, "Rethinking positional encoding in language pre-training," arXiv preprint arXiv:2006.15595, 2020.
- [44] S. Khan, M. Naseer, M. Hayat, S. W. Zamir, F. S. Khan, and M. Shah, "Transformers in vision: A survey," ACM Computing Surveys (CSUR), 2021.
- [45] A. F. Agarap, "Deep learning using rectified linear units (relu)," arXiv preprint arXiv:1803.08375, 2018.
- [46] J. L. Ba, J. R. Kiros, and G. E. Hinton, "Layer normalization," arXiv preprint arXiv:1607.06450, 2016.
- [47] C. Kirschbaum, K.-M. Pirke, and D. H. Hellhammer, "The 'trier social stress test'—a tool for investigating psychobiological stress responses in a laboratory setting," *Neuropsychobiology*, vol. 28, no. 1-2, pp. 76–81, 1993.
- [48] D. Makowski, T. Pham, Z. J. Lau, J. C. Brammer, F. Lespinasse, H. Pham, C. Schölzel, and S. Chen, "Neurokit2: A python toolbox for neurophysiological signal processing," *Behavior research meth-ods*, vol. 53, no. 4, pp. 1689–1696, 2021.
- [49] E. Haapalainen, S. Kim, J. F. Forlizzi, and A. K. Dey, "Psychophysiological measures for assessing cognitive load," in *Proceed*ings of the 12th ACM international conference on Ubiquitous computing, 2010, pp. 301–310.
- [50] T. Zhou and J. P. Wachs, "Early prediction for physical human robot collaboration in the operating room," *Autonomous Robots*, vol. 42, no. 5, pp. 977–995, 2018.

- [51] G. Shafer, "Dempster-shafer theory," Encyclopedia of artificial intelligence, vol. 1, pp. 330–331, 1992. [52] A. Graves, "Long short-term memory," in Supervised sequence
- labelling with recurrent neural networks. Springer, 2012, pp. 37–45.
- [53] F. Scarselli, M. Gori, A. C. Tsoi, M. Hagenbuchner, and G. Monfardini, "The graph neural network model," IEEE transactions on neural networks, vol. 20, no. 1, pp. 61-80, 2008.
- [54] T. Song, W. Zheng, P. Song, and Z. Cui, "Eeg emotion recognition using dynamical graph convolutional neural networks, Transactions on Affective Computing, vol. 11, no. 3, pp. 532–541, 2018.
- [55] P. Zhong, D. Wang, and C. Miao, "Eeg-based emotion recognition using regularized graph neural networks," IEEE Transactions on Affective Computing, 2020.
- [56] J. Sun, J. Xie, and H. Zhou, "Eeg classification with transformerbased models," in 2021 IEEE 3rd Global Conference on Life Sciences and Technologies (LifeTech). IEEE, 2021, pp. 92-93.
- [57] S. J. Russell, Artificial intelligence a modern approach. Pearson Education, Inc., 2010.
- J. Gareth, W. Daniela, H. Trevor, and T. Robert, An introduction to statistical learning: with applications in R. Spinger, 2013.
- [59] C. M. Bishop and N. M. Nasrabadi, Pattern recognition and machine learning. Springer, 2006, vol. 4, no. 4.
 [60] K. Hou, G. Shao, H. Wang, L. Zheng, Q. Zhang, S. Wu, and W. Hu,
- "Research on practical power system stability analysis algorithm based on modified svm," Protection and Control of Modern Power Systems, vol. 3, no. 1, pp. 1–7, 2018.
 [61] Y. Wu and Y. Liu, "Robust truncated hinge loss support vector
- machines," Journal of the American Statistical Association, vol. 102, no. 479, pp. 974-983, 2007.
- [62] Y. Bian, J. Huang, X. Cai, J. Yuan, and K. Church, "On attention redundancy: A comprehensive study," in Proceedings of the 2021 Conference of the North American Chapter of the Association for Computational Linguistics: Human Language Technologies, 2021, pp. 930-945.
- [63] S. Bhojanapalli, A. Chakrabarti, A. Veit, M. Lukasik, H. Jain, F. Liu, Y.-W. Chang, and S. Kumar, "Leveraging redundancy in attention with reuse transformers," arXiv preprint arXiv:2110.06821, 2021.
- [64] A. Zeyer, P. Bahar, K. Irie, R. Schlüter, and H. Ney, "A comparison of transformer and lstm encoder decoder models for asr," in 2019 IEEE Automatic Speech Recognition and Understanding Workshop (ASRU). IEEE, 2019, pp. 8-15.

APPENDIX A HYPER-PARAMETERS OF THE Husformer

TABLE 9: Hyper-parameters of the *Husformer* utilized for each experiment

Parameter name	Raw DEAP	Preprocessed DEAP	WESAD	Raw MOCAS	Preprocessed MOCAS	Cogload
Batch Size	1024	1024	512	64	128	1024
Initial Learning Rate	2e-3	2e-3	1e-3	1e-3	1e-3	1e-3
Optimizer	Adam	Adam	Adam	Adam	Adam	Adam
Transformer Hidden Unit Size	40	40	40	40	40	40
Crossmodal Attention Heads	3	3	3	5	5	3
Crossmodal Attention Block Dropout	0.1	0.1	0.05	0.05	0.05	0.1
Output Dropout	0.1	0.1	0.1	0.1	0.1	0.1
Epochs	20	20	60	40	40	80

APPENDIX B CLASSIFICATION RESULTS USING EACH SINGLE MODALITY

TABLE 10: Best performing classification results of using single modality on the raw DEAP and preprocessed DEAP Dataset in terms of multi-class average accuracy (Acc) and multi-class average F1-score (F1) with stand deviations. All best performing results are obtained with the transformer network.

Dataset		Raw l	DEAP		Preprocessed DEAP			
Criteria	Valence		Aro	usal	Valence Arousa		usal	
Metric	$Acc(\%)^h$	$F1(\%)^h$	$Acc(\%)^h$	$F1(\%)^h$	$Acc(\%)^h$	$F1(\%)^h$	$Acc(\%)^h$	$F1(\%)^{h}$
EEG	78.73±1.84	78.86 ± 2.01	79.20±1.53	79.64 ± 1.74	90.91±1.21	91.02±1.23	90.79±0.11	90.79 ± 0.61
EMG	71.39 ± 2.12	71.44 ± 2.07	72.05 ± 1.98	72.39 ± 1.57	83.42±0.78	83.44 ± 0.76	80.82 ± 0.63	80.80 ± 0.60
EOG	52.80 ± 1.74	51.79 ± 1.64	54.08 ± 1.38	56.78 ± 1.25	68.57±1.66	71.38 ± 1.26	70.23 ± 0.25	71.24 ± 0.20
GSR	50.94±2.34	51.39 ± 2.16	52.46±2.11	53.83 ± 1.95	67.41±0.94	65.50 ± 0.75	68.51 ± 0.69	63.04 ± 0.66

TABLE 11: Best performing classification results of using single modality on the raw MOCAS and preprocessed MOCAS Dataset in terms of multi-class average accuracy (Acc) and multi-class average F1-score (F1) with stand deviations; \clubsuit : classification with Transformer, and \spadesuit : classification with GCN.

Dataset	Raw M	IOCAS	Preprocessed MOCAS		
Metric	$Acc(\%)^h$	$F1(\%)^h$	$Acc(\%)^h$	$F1(\%)^{h}$	
EEG	40.51±0.43♠	40.35±0.39♠	51.14±0.23	52.55±0.23♠	
EEG_POW	74.37±1.17♣	73.99±1.31♣	91.10±1.60♣	91.02±1.58♣	
GSR	39.51±0.42♠	41.40±0.45♠	49.25±0.38♣	52.79±0.34♣	
BVP	48.78±1.42♠	49.72±1.50♣	77.41±1.82♣	77.37±1.85♣	
EAR	51.55±2.99♣	53.50±2.16♣	55.67±0.29♣	52.58±0.32♣	

TABLE 12: Best performing classification results of using single modality on the (a) WESAD Dataset and (b) CogLoad Dataset in terms of multi-class average accuracy (*Acc*) and multi-class average F1-score (*F*1) with stand deviations. •: classification with Transformer; •: classification with GCN.

	(a)		(b)			
Dataset	WES	SAD	Dataset	Cogload		
Metric	$Acc(\%)^h$	$F1(\%)^h$	Metric	$Acc(\%)^h$	$F1(\%)^{h}$	
EMG	56.92±0.33♠	59.83±0.41♠	GSR	62.38±0.54	63.45±0.61	
EDA	58.06±0.64♣	60.66±0.39♠	HR	36.47±0.94♠	35.96±1.02♠	
BVP	64.96±0.82♣	65.48±0.86♣	RR	45.81±2.13♠	48.51±2.28♣	
RESP	68.30±1.07♣	70.06±0.91♣	ACC	40.52±1.62♠	39.28±1.34♠	